THE ASTROPHYSICAL JOURNAL, 398:L1–L4, 1992 October 10

A DEGREE-SCALE MEASUREMENT OF ANISOTROPY OF THE COSMIC BACKGROUND RADIATION

TODD GAIER, JEFFREY SCHUSTER, JOSHUA GUNDERSEN, TIMOTHY KOCH,
MICHAEL SEIFFERT, PETER MEINHOLD, AND PHILIP LUBIN
Department of Physics, University of California at Santa Barbara, Santa Barbara, CA 93106
Received 1992 March 23; accepted 1992 July 24

ABSTRACT

We report on the preliminary result of a search for anisotropy in the cosmic background radiation (CBR) with a beam size of $\approx 1\overset{\circ}{.}5$ FWHM over a wavelength range of 8–12 mm. The system operated successfully for 500 hr at the South Pole during the 1990–1991 austral summer. The data from one region, representing 25 hr after editing, are presented here. A strong signal is present in the lower frequency channels with a spectrum unlike CBR fluctuations, and is probably due to foreground emission. The highest frequency channel has the smallest contribution from this signal and has been used to set a 95% confidence level upper limit of $\Delta T/T \leq 1.4 \times 10^{-5}$ for fluctuations with a Gaussian autocorrelation function at a coherence angle of $1\overset{\circ}{.}2$. This is significantly more sensitive than previous experiments at this angular scale.

Subject headings: cosmology: cosmic microwave background

1. INTRODUCTION

Spatial anisotropies of the cosmic background radiation (CBR) provide a critical test for cosmological theories. Current upper limits are $\Delta T/T \leq 1.8 \times 10^{-5}$ at arcminute scales (Readhead et al. 1989, hereafter OVRO), 3.5×10^{-5} at $0\overset{\circ}{.}5$ (Meinhold & Lubin 1991, hereafter ACME-SIS), and 1.6×10^{-5} at 10° and larger scales (Meyer, Cheng, & Page 1991, hereafter MIT). At $1\overset{\circ}{.}2$, the previous upper limit was $\Delta T/T \leq 1 \times 10^{-4}$ (Timbie & Wilkinson 1990, hereafter T&W).

Measurements at scales of a few degrees are of special interest, as they probe structure of horizon size at decoupling, as well as test theories of structure formation with significant reionization. CBR fluctuations of this scale arise largely via the Sachs-Wolfe effect (Sachs & Wolfe 1967) and provide a direct probe of $\delta\rho/\rho$ at $z_{\rm dec}$. Anisotropy measurements at this scale can be compared with other measurements of large-scale structure as a test of cosmological models (Juszkiewicz, Górski, & Silk 1987; Górski 1992).

Standard cold dark matter (CDM) models predict significant structure in the CBR on scales of arcminutes to degrees, depending on the model. The angular scale of primordial fluctuations is expected to increase for $z_{\rm rec} \ll 1100$. For an ionized universe, CDM predicts significant structure on scales of 1°–2° at a level $\Delta T/T \geq 1 \times 10^{-5}$ (Bond & Efstathiou 1987; Bond et al. 1991).

At this level of sensitivity, experiments performed at any wavelength are expected to detect signals from confusing sources. These include foreground Galactic emission, extragalactic discrete sources, terrestrial atmospheric signals, and sidelobe pickup (Franceschini et al. 1989). Accordingly, it has become necessary to obtain more information than monochromatic measurements of anisotropy can provide. Simultaneous measurements at several frequencies can, in principle, allow one to distinguish between intrinsic CBR fluctuations and confusing foreground sources.

2. THE EXPERIMENT

The experiment used the University of California at Santa Barbara (UCSB) Advanced Cosmic Microwave Explorer (ACME) off-axis Gregorian telescope described in previous publications (Meinhold & Lubin 1991; Meinhold et al. 1992a). The reader should refer to these papers for many of the experimental details.

The significant difference between the previous experiments and this one is the detector. We use a broad-band high electron mobility transistor (HEMT) amplifier cooled to ≈ 6 K in a ^{4}He cryostat. The amplifier operates from 25 to 35 GHz (8–12 mm) with a receiver noise temperature of about 30 K. The band is split into four 2.5 GHz bands using an array of circulators and waveguide filters. Splitting the band provides spectral information on any signals detected. The receiver schematic is shown in Figure 1. Channels 1–4 correspond to low-frequency to high-frequency channels, respectively. A fifth channel monitored the full band, and is used as a diagnostic tool. The HEMT amplifier is attached directly to a cooled scalar horn which feeds the optics.

The optical arrangement results in a $1\overset{\circ}{.}65$ (Gaussian FWHM) beam measured at a frequency of 27.7 GHz. The beam is expected to vary as

$$\theta_{\rm FWHM}(\nu) = 1\overset{\circ}{.}65 \pm 0\overset{\circ}{.}1 \times \left(\frac{27.7}{\nu_{\rm GHz}}\right).$$

The beamwidth of channel 4 is expected to be $1\overset{\circ}{.}4$, consistent with Moon scans. Low sidelobe response is critical in this experiment and has been measured to be less than 10^{-6} for angles greater than 30° from bore sight. The beam is chopped at 8 Hz by nutating the secondary mirror with a resonant counterrotating servo motor. The beam is thrown sinusoidally with an amplitude of $1\overset{\circ}{.}5$ on the sky. This angle is limited by both the chopper mechanism and the sidelobe requirements.

The signals out of the detector diodes are fed into synchronous detectors with ideal integrator output filters (integration time = 1.25 s) and are then digitized. After synchronous detection, the instrument point-source response is antisymmetric, with the peaks separated by $2\overset{\circ}{.}1$ on the sky. The entire telescope sits on a rotation table which, in this configuration, points the beam to a relative accuracy of better than 5′.

The chopped noise that we expect from this system is between 1.35 and 1.6 mK $s^{1/2}$ (1 σ) for the different channels.

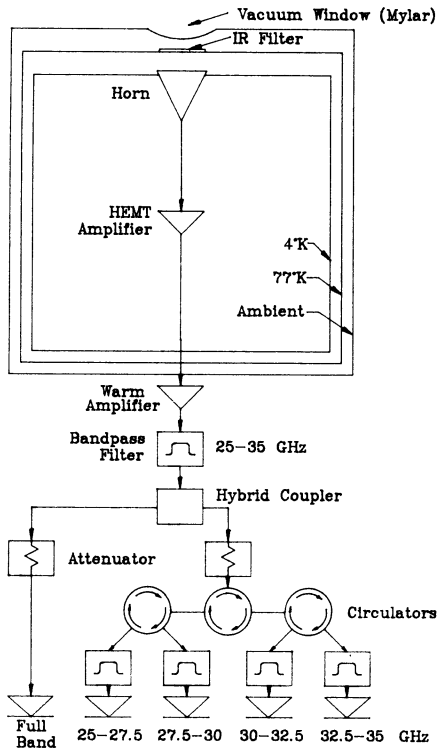

FIG. 1.—Receiver schematic. This includes RF components from the feed horn to the detector diodes. Not included are isolators at the output of the four final bandpass filters.

When shot noise from the atmosphere and CBR is included, the noise should be between 1.6 and 2.2 mK $s^{1/2}$. During this run the actual noise varied between 1.8 and 4.5 mK $s^{1/2}$ in the lowest noise channel, depending upon the atmospheric conditions.

3. OBSERVATION STRATEGY

A discrete scan strategy similar to that of previous work (Meinhold & Lubin 1991) was adopted. This scan consists of moving the telescope in azimuth by steps corresponding to 2°.1 steps on the sky in order to overlap the chopped beams. This technique takes advantage of the topographic location of the South Pole, to track in right ascension without changing elevation. This minimizes possible atmospheric or gravitational offsets, as well as eliminating the problem of beam rotation.

An N point scan will sample a region $2°.1 \times (N + 1)$ across the sky. We examined the low-frequency (408 MHz) map of Haslam et al. (1982) and the *IRAS* 100 μm map to determine a nominal scan size and location that would be relatively free from Galactic synchrotron and dust emission. Simulations of the instrument response on these maps showed that in a clean region of the sky typical signals of 20 μK (rms) would be seen at 30 GHz over a 20° scan. For scans larger than this, greater Galactic signals are expected.

For this reason, a 9 point scan was chosen. Because of possible Galactic contamination, we felt it would be desirable to build a two-dimensional map of the region. The map consists of 6 scans of 9 points each separated in elevation by 0°.75, centered at $\alpha = 0^h.5$, $\delta = -61°.9$. The Sun was at an angle $\geq 68°$ in azimuth from the edges of the map during the observation. In addition, we performed a deep 13 point scan and a 15 point scan overlapping the map region. To test the system sensitivity to small signals, a Galactic plane crossing and a 9 point scan of the Large Magellanic Cloud (LMC) were performed.

The system was calibrated one or two times a day by inserting a warm target into the beam. The calibration in channel 1 varied by $\pm 5.5\%$ (1 σ) during the entire measurement period, while the variation in channels 2–4 was less than $\pm 3.2\%$. The mean calibration for the full data-taking period is used throughout the analysis. The calibration and beam were also tested by detailed scans of the Moon. The actual measured Moon signal was about 25% smaller than predicted by a lunar emission model (Keihm 1983). We consider this error acceptable, as the measurement was made at low elevation (below 15°), where atmospheric attenuation becomes significant.

The instrument collected data for a total of about 500 hr during the 1990–1991 South Pole summer. After editing for bad weather and system faults, about 150 hr remain. The data presented here are from a 9 point scan near the center of the map ($\delta = -62°.25$). This scan had the longest total integration time in the 9 point by 6 elevation map and was expected to be relatively free from diffuse Galactic contamination. This scan represents 120 hr of total data and 25 hr of edited data. The remainder of the data will be presented at a later date.

4. DATA EDITING AND REDUCTION

The data were edited in the following manner. First, outliers were removed from the raw data (points deviating by more than 5 σ in a 20 s sample). This removed less than 1% of the total data. The data were then binned into scan positions of constant right ascension, eliminating the 10% of the data which fell between scan positions.

Occasionally, the chopper became unstable or varied in amplitude. This had the effect of distorting the beam on the sky and possibly changing the reference signal to the lock-in amplifiers. For this reason the chopper was monitored, and when the amplitude or zero position fell outside a specified range, all data were removed.

We define a full scan as starting at position 1 and ending at position 1. A half-scan starts at position 1 and ends at position 9. The raw data at each position are of the approximate form

$$\Delta_i = T_{\gamma_i + \alpha/2} - T_{\gamma_i - \alpha/2} .$$

This is the usual single difference form, where α is the chop angle, 2°.1. T_{γ_i} is the CBR temperature at angle γ_i, convolved with our beam.[1]

The data were divided into half-scans, and a line was fitted to the data as a function of time in each half-scan. This had the effect of removing any line in right ascension from the final data set. The resulting approximate form of the data is

$$\Delta_i' = \Delta_i - (\gamma_i m + b) .$$

The values m and b are the slope and offset given by a least-squares fit to the data Δ_i. The removal of the line only affects our sensitivity at angular scales large compared with our beam. The typical size of the removed signal was ≈ 250 μK (to a maximum of 800 μK) between points 1 and 9, and was similar in all channels. Partial half-scans were totally removed. An error window was defined for elevation at $\pm 7'.2$ (the elevation was not servoed to correct for wind).

[1] The effective beamwidth is actually larger in one dimension due to the sinusoidal chop. A factor of 1.08 is applied to FWHM to correct for this.

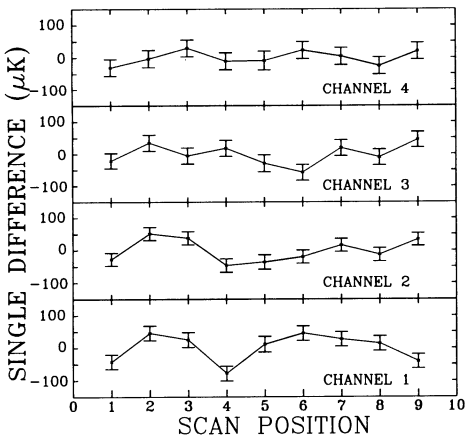

FIG. 2.—Data from $\delta = -62^\circ.25$. Channel 1 refers to the band 25–27.5 GHz. Channel 4 refers to 32.5–35 GHz. A linear component in scan position has been removed. Scan positions are separated by 2°.1 on the sky. Scan position 5 corresponds to $\alpha = 0^h.5$. The data are in units of μK *thermodynamic*. The error bars displayed are $\pm 1\ \sigma$. The data are also shown in Table 1.

The single largest source of data loss was bad weather. Even though the South Pole is an excellent observation site with exceptionally low precipitable H_2O content,[2] at times of cloudy skies the noise could increase by a factor of 10. The noise distribution has significant non-Gaussian tails as expected from the weather. For each channel the distribution of $\frac{1}{2}$ scan rms's (after fitting) is cut at a value such that above this value, the final error bar increases. This value is 3.2, 2.8, 3.6, and 3.4 mK $s^{1/2}$ for channels 1–4, respectively. Seventy percent of the data from the 5 days of the observations of $\delta = -62^\circ.25$ were removed this way.

The data were then binned into right ascension, and a final average and standard deviation were calculated. These data from all four channels are displayed in Figure 2 and Table 1.

5. DATA ANALYSIS

Prior to binning, the data between channels are partially correlated. The correlation coefficient ρ for these data is between 0.21 and 0.32 depending on the channels in question, and does not vary significantly as a function of scan position. Such correlations are expected, since all channels are observing through the same slice of atmosphere simultaneously.

The correlated component is about the right size to explain the excess short-term noise in the data, arising from chopped atmospheric signals. If atmospheric fluctuations are random in time, no net signal results and the data in the four channels will appear correlated but explained by the errors. For analysis of a single channel, correlations are unimportant. They are important, however, in any spectral analysis of the data and the determination of the degree of atmospheric contamination.

An obvious feature of the data in Figure 2 is the large correlated signal in channels 1 and 2. The signal also drops sharply as a function of frequency, as expected for synchrotron or bremsstrahlung emission. Considerable spectral analysis has been performed on this data set. A model where the most probable signals have a CBR spectrum (for Gaussian fluctuations at 1°.2) is accepted with 2% probability.

Since channel 4 should have the least foreground contamination, we use it as a measure of CBR signals. If foreground signals can effectively be removed, the other channels could provide greater sensitivity. For comparison, the reduced χ^2 of the channel 4 data set is 0.74 for $\nu = 7$ degrees of freedom.

[2] The atmospheric water content was typically below 1 mm during the observation period, becoming as high as 3 mm during inclement weather.

TABLE 1

$\delta = -62^\circ.15'$, $\alpha = 0^h.5$ DATA SET

SCAN POSITION	BIN AVERAGES (μK $\pm$ 1 σ)			
	Channel 1	Channel 2	Channel 3	Channel 4
1.....	−42.6 ± 22.1	−27.6 ± 19.8	−20.7 ± 23.9	−30.5 ± 25.9
2.....	45.6 ± 22.4	51.7 ± 20.3	35.1 ± 24.8	−3.2 ± 26.5
3.....	25.1 ± 23.0	38.1 ± 20.5	−5.3 ± 25.0	29.2 ± 26.1
4.....	−78.2 ± 22.6	−46.6 ± 20.6	18.2 ± 24.9	−10.8 ± 26.3
5.....	11.4 ± 23.9	−36.2 ± 22.2	−28.9 ± 26.5	−8.7 ± 28.8
6.....	45.1 ± 22.4	−19.9 ± 20.3	−57.5 ± 24.9	23.1 ± 26.4
7.....	26.8 ± 22.3	15.6 ± 20.3	19.2 ± 24.7	4.7 ± 26.5
8.....	13.8 ± 22.6	−13.5 ± 20.1	−9.7 ± 24.6	−24.7 ± 26.6
9.....	−41.0 ± 21.8	33.5 ± 19.8	44.5 ± 23.9	20.3 ± 25.8

NOTE.—Scan positions are in steps of 2°.1 on the sky. Scan position 5 corresponds to $\alpha = 0^h.5$. Bin average is the mean of all data at that scan position after fitting. Units are μK for a 2.73 K blackbody. The data are displayed in Fig. 2.

A Monte Carlo analysis similar to that used in the ACME-SIS result was employed in order to set upper limits to CBR fluctuations using only channel 4. CBR fluctuations can be characterized by their autocorrelation function (ACF),

$$\left\langle \frac{T_{\gamma_i}}{T_0} \frac{T_{\gamma_j}}{T_0} \right\rangle = C(\Theta) ,$$

where $\gamma_j - \gamma_i = \Theta$. We determined 95% confidence level upper limits to the rms CBR fluctuations with a Gaussian ACF,

$$C(\Theta) = C_0 \exp\left[-\Theta^2/(2\Theta_c^2)\right] .$$

Three thousand random maps were generated with the above ACF for each value of Θ_c tested. The rms of the assumed sky fluctuations, $C_0^{1/2}$, was varied, and the full experimental response simulated on each sky. Any linear trend in the data was removed, and the same statistical analysis that was used in the ACME-SIS result was employed to set an upper limit. We found this upper limit to be $C_0^{1/2} \leq 1.4 \times 10^{-5}$ at $\Theta_c = 1^\circ.2$. The power of the test was 40%, and we assume $T_0 = 2.73$ K (Mather et al. 1990).

Additionally, we performed likelihood analysis on the data using the full form of the correlation matrix, including off-diagonal terms (Vittorio et al. 1991; Bond et al. 1991). This form of the likelihood function is given by

$$L(C_0, \Theta_c) \equiv (2\pi)^{-N/2} |\boldsymbol{M}|^{-1/2} \exp\left(-\tfrac{1}{2} \sum_{i=1}^{N} \sum_{j=1}^{N} \Delta_i' \boldsymbol{M}_{ij}^{-1} \Delta_j' \right) .$$

The need for extensive simulations is eliminated by writing the theoretical correlation matrix, $\boldsymbol{M}(C_0, \Theta_c)$, in terms of theoretical data, $\langle \Delta_i' \Delta_j' \rangle$, instead of $\langle \Delta_i \Delta_j \rangle$.[3] So

$$\boldsymbol{M}_{ij} = \langle \Delta_i' \Delta_j' \rangle_{\rm th} + \delta_{ij} \sigma_i^2 .$$

$\langle \Delta_i' \Delta_j' \rangle_{\rm th}$ is derived using $\langle T_{\gamma_i} T_{\gamma_j} \rangle_{\rm th} = T_0^2\, C(\Theta, \Theta_c, C_0, \sigma_b)$, the beam convolved (where σ_b is the σ of our beam for a Gaussian fit) correlation function with $\gamma_j - \gamma_i = \Theta = |j - i|\alpha$; σ_i is the error bar at position i. The actual upper limits to $C_0^{1/2}$ are set using the integrated area under the resulting likelihood

[3] The diagonal form $\langle \Delta^2 \rangle = 2T_0^2[C(0) - C(\alpha)]$ is inadequate because of the overlapping beams in the scan strategy.

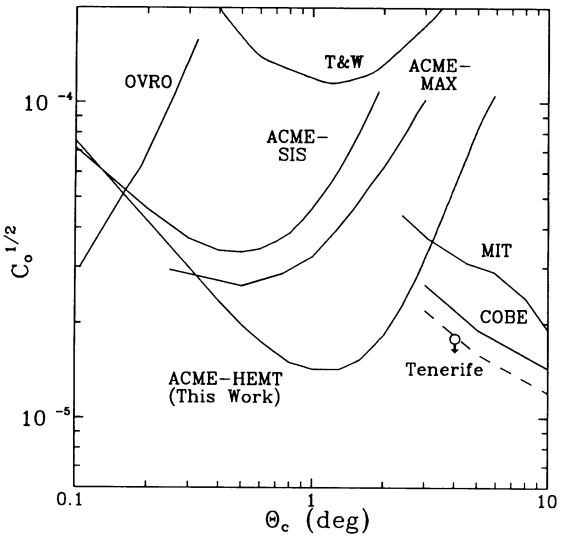

FIG. 3.—95% confidence level limits to the rms amplitude of CBR fluctuations assuming a Gaussian autocorrelation function. All curves are upper limits except for the dashed line, which is the *COBE* lower limit (Wright et al. 1992). The recent Tenerife upper limit at 4° is given by the open circle with attached arrow. The ACME-HEMT upper limits are set using the data of channel 4 in Fig. 2 by integrating the area under the likelihood curve as described in the text.

curve. This 95% confidence level limit of 39 μK agrees with the previous Monte Carlo analysis and is displayed in Figure 3 for a range of Θ_c tested.

We also found the 95% confidence level upper limits to $C_0^{1/2}$ implied by the other channels. These are 102, 85, and 65 μK for channels 1–3, respectively. A simple co-addition of channels 1–4 results in an upper limit of 53 μK. A similar analysis combining only channels 3 and 4 gives an upper limit of 43 μK.

This result represents a factor of 7 improvement in sensitivity over previous limits to the anisotropy of the CBR at 1°.2 (Timbie & Wilkinson 1990). At smaller angles, the limits are lower than the previous ACME-SIS upper limit at $\Theta_c = 0°.5$. At larger angles the sensitivity drops rapidly. These results are also included in Figure 3.

Since this paper was submitted, several new results have been released. We have included some of these limits in Figure 3. They include the recent detection of anisotropy by the *COBE* satellite (Wright et al. 1992), a limit set by the MAX experiment (Devlin et al. 1992; Meinhold et al. 1992b [ACME-MAX in Fig. 3]), and a recent upper limit set by the Tenerife experiment (Watson et al. 1992).

6. CONCLUSION

We have made a sensitive map of anisotropy of the CBR at multiple frequencies. One elevation from this map, the most sensitive, has been analyzed. The lower frequencies have strong detections, while the higher frequencies do not. This type of spectrum is not indicative of CBR fluctuations. The data in channel 4 (32.5–35 GHz) imply a 95% confidence level upper limit of $\Delta T/T \leq 1.4 \times 10^{-5}$ for Gaussian fluctuations in the CBR. This is substantially lower than previous limits at 1°–2°.

Work is proceeding on the analysis of the entire map region as well as the larger scans. The ultimate sensitivity of the entire data set should be $\Delta T/T \leq 8 \times 10^{-6}$ (2 σ), and even better if contaminating sources can be removed.

This project would not have been possible without the Center for Particle Astrophysics and the support and encouragement of Bernard Sadoulet. The cryogenic HEMT amplifier was supplied by Mike Balister and Marian Pospiezalski at NRAO. Lyman Page provided helpful comments at the South Pole and later. Conversations with Dick Bond, Kris Górski, Joe Silk, and Nicola Vittorio were helpful during the analysis. This work was supported by the National Aeronautics and Space Administration under grant NAGW-1062; the National Science Foundation under Polar grant NSF DPP 89-20578; and the Center for Particle Astrophysics under grant NSF UCB AST88-0916. Finally, we would again like to thank Bill Coughran and the entire ASA staff for their support at the South Pole during the 1990–1991 austral summer.

REFERENCES

Bond, J. R., & Efstathiou, G. 1987, MNRAS, 226, 655
Bond, J. R., Efstathiou, G., Lubin, P. M., & Meinhold, P. R. 1991, Phys. Rev. Lett., 66, 2179
Devlin, M., et al. 1992, in Proc. NAS Colloquium on Physical Cosmology (Irvine), in press
Franceschini, A., Toffolatti, L., Danese, A., & De Zotti, G. 1989, ApJ, 344, 35
Górski, K. M. 1992, ApJ, 398, L5
Haslam, C. G. T., Salter, C. J., Stoffel, H., & Wilson, W. E. 1982, A&AS, 47, 1
Juszkiewicz, R., Górski, K., & Silk, J. 1987, ApJ, 323, L1
Keihm, S. J. 1983, JPL Internal Memo, 1983 May 2
Mather, J. C., et al. 1990, ApJ, 354, L37
Meinhold, P. R., & Lubin, P. M. 1991, ApJ, 370, L11 (ACME-SIS)
Meinhold, P. R., et al. 1992a, ApJ, submitted
Meinhold, P. R., et al. 1992b, in preparation
Meyer, S. S., Cheng, E. S., & Page, L. A. 1991, ApJ, 371, L1 (MIT)
Readhead, A. C. S., Lawrence, C. R., Myers, S. T., Sargent, W. L. W., Hardebeck, H. E., & Moffet, A. T. 1989, ApJ, 346, 566 (OVRO)
Sachs, R., & Wolfe, A. 1967, ApJ, 147, 73
Timbie, P. T., & Wilkinson, D. T. 1990, ApJ, 353, 140 (T&W)
Vittorio, N., Meinhold, P. R., Muciaccia, P. F., Lubin, P. M., & Silk, J. 1991, ApJ, 372, L1
Watson, R. A., et al. 1992, Nature, 357, 660
Wright, E. L. 1992, ApJ, 396, L13